Available online at www.sciencedirect.com
SCIENCE DIRECT®
Biomaterials 25 (2004) 4149–4161
Biomaterials
www.elsevier.com/locate/biomaterials

Design of porous scaffolds for cartilage tissue engineering using a three-dimensional fiber-deposition technique

T.B.F. Woodfield[a,b,*], J. Malda[a,b], J. de Wijn[b], F. Péters[b], J. Riesle[b], C.A. van Blitterswijk[a,b]

[a] *Institute for Biomedical Technology, University of Twente, P.O. Box 217, Enschede 7500 AE, The Netherlands*
[b] *IsoTis S.A., Prof. Bronkhorstlaan 10-D, Bilthoven 3723 MB, The Netherlands*

Received 1 September 2003; accepted 21 October 2003

Abstract

In this study, we present and characterize a fiber deposition technique for producing three-dimensional poly(ethylene glycol)-terephthalate—poly(butylene terephthalate) (PEGT/PBT) block co-polymer scaffolds with a 100% interconnecting pore network for engineering of articular cartilage. The technique allowed us to ''design-in'' desired scaffold characteristics layer by layer by accurately controlling the deposition of molten co-polymer fibers from a pressure-driven syringe onto a computer controlled $x-y-z$ table. By varying PEGT/PBT composition, porosity and pore geometry, 3D-deposited scaffolds were produced with a range of mechanical properties. The equilibrium modulus and dynamic stiffness ranged between 0.05–2.5 and 0.16–4.33 MPa, respectively, and were similar to native articular cartilage explants (0.27 and 4.10 MPa, respectively).

3D-deposited scaffolds seeded with bovine articular chondrocytes supported a homogeneous cell distribution and subsequent cartilage-like tissue formation following in vitro culture as well as subcutaneous implantation in nude mice. This was demonstrated by the presence of articular cartilage extra cellular matrix constituents (glycosaminoglycan and type II collagen) throughout the interconnected pore volume. Similar results were achieved with respect to the attachment of expanded human articular chondrocytes, resulting in a homogenous distribution of viable cells after 5 days dynamic seeding.

The processing methods and model scaffolds developed in this study provide a useful method to further investigate the effects of scaffold composition and pore architecture on articular cartilage tissue formation.

Keywords: Cartilage tissue engineering; Chondrocyte; Porosity; Rapid prototyping; Scaffold

1. Introduction

The main function of articular cartilage is to provide a smooth, near frictionless articulating surface while mediating the transfer of load within the joint to the underlying subchondral bone [1]. When damaged, however, the regenerative capacity of articular cartilage remains limited in comparison with other musculoskeletal tissues such as bone and muscle [2]. Although numerous treatment protocols are currently employed clinically, few approaches, if any, exist which are capable of consistently restoring long-term function to damaged articular cartilage [3,4]. Tissue engineering approaches adopting scaffold conduits for delivery or recruitment of reparative cells in an organized manner to bridge voids within cartilage defects, offer considerable promise as repair strategies [5,6].

Scaffolds designed for use in cell-based therapies to repair damaged articular cartilage should ideally provide the following characteristics: (i) a three-dimensional (3D) and highly porous structure to support cell attachment, proliferation and extra-cellular matrix (ECM) production; (ii) an interconnected/permeable pore network to promote nutrient and waste exchange; (iii) a biocompatible and bioresorbable substrate with controllable degradation rates; (iv) a suitable surface chemistry for cell attachment, proliferation, and differentiation; (v) mechanical properties to support, or match, those of the tissues at the site of implantation;

*Corresponding author. IsoTis S.A., Prof. Bronkhorstlaan 10-D, Bilthoven 3723 MB, The Netherlands. Tel.: +31-30-229-5121; fax: +31-30-228-0255.
E-mail address: tim.woodfield@isotis.com (T.B.F. Woodfield).

0142-9612/$ - see front matter © 2003 Elsevier Ltd. All rights reserved.
doi:10.1016/j.biomaterials.2003.10.056

(vi) an architecture which promotes formation of the native anisotropic tissue structure; and (vii) a reproducible architecture of clinically relevant size and shape [3,7–11]. Yet most scaffolds reported to date for cartilage repair conform to only a few of these criteria.

Scaffold processing techniques used to date have focused on the development of porous materials via fiber bonding, solvent casting, particulate leaching, membrane lamination, melt molding, temperature-induced phase separation, and gas foaming [12,13]. The control over scaffold architecture using these fabrication techniques, however are highly process driven, and not design driven. As a result, investigators have recently turned to rapid prototyping (RP) techniques for producing porous scaffolds for tissue engineering applications [8,14–17]. RP is a subset of mechanical processing techniques which allows highly complex, but reproducible structures, to be constructed one layer at a time via computer-aided design (CAD) models and computer-controlled tooling processes (CAM). These techniques essentially allow researchers to design-in desired properties, such as porosity, interconnectivity and pore size, in a number of polymer and ceramic materials. RP methodologies studied to date have included stereolithography, selective laser sintering, ballistic particle manufacturing and 3D printing [12], using highly specialized polymers and materials designed specifically to meet the processing requirements of each RP system. However, the transfer of RP technologies to encompass biocompatible and bioresorbable materials still poses a significant challenge, particularly in developing 3D scaffolds for tissue engineering applications.

Hutmacher and co-workers have developed scaffolds primarily for bone tissue engineering applications based on fused deposition modeling (FDM) of poly(ε-caprolactone) (PCL) polymers [8,12,14,16,17]. This process uses rollers to feed a pre-formed fiber through a heated nozzle onto a computer-controlled table. PCL was chosen due to its relatively low melting temperature (−60°C) and thermal stability at high temperatures [14]. Drawbacks of the FDM technique include the need for pre-formed fibers with specific size and material properties to feed through the rollers and nozzle. As a result, FDM has a narrow processing window [18], and its use with biodegradable polymer systems other than PCL have not been reported. More recently, computer-guided 3D plotting techniques have been developed [18–22] which use a pressurized syringe to produce scaffolds with complex geometries and a wider range of processing capability, i.e. agar, agarose materials at room temperature as well as hot melts from low viscosity polymers.

At present, we are evaluating a series of amphiphilic, biodegradable poly(ether ester) multiblock co-polymers as carrier materials for articular cartilage repair. These thermoplastic elastomers are based on hydrophilic poly(ethylene glycol)-terephthalate (PEGT) and hydrophobic poly(butylene terephthalate) (PBT) blocks. A major advantage of these types of co-polymer systems is that by varying the amount and the length of the two building blocks, an entire family of polymers can be obtained. This offers extensive possibilities in the design of systems with tailor-made properties, such as swelling, degradability and mechanical strength [23–25]. The addition of 0.2 wt% α-tocopherol as an antioxidant provides stability to the PEGT/PBT co-polymers at elevated temperatures; thus, providing suitable viscosities to support a wide range of processing techniques. Various in vitro and in vivo studies have demonstrated both the biocompatibility and biodegradable nature of PEGT/PBT co-polymers [24,26–28] and are currently applied for a range of biomedical applications [7,29–32]. Degradation occurs via both hydrolysis (cleavage of ester bond linking ester and hydrophilic ether segments) and oxidation (PEG chain scission via free-radical reactions), and in both cases, degradation is more rapid for copolymers with high PEG content [26]. The attachment, proliferation, morphology, and differentiation state of chondrocytes has also been demonstrated on different compositions of 2D PEGT/PBT films [31]. Controlled release of bioactive factors from these materials has also been demonstrated [7,33].

Few investigators have produced scaffolds for articular cartilage tissue engineering applications using RP or evaluated in vitro and in vivo tissue formation on such scaffolds. Further development of RP technologies offer promising avenues to generate scaffolds which meet a large number of the scaffold requirements explained previously. Therefore, the purpose of this study was to evaluate a model 3D-deposition system for producing porous PEGT/PBT scaffolds. The mechanical properties of various scaffolds were assessed for comparison with normal articular cartilage and results following in vitro and in vivo tissue culture are reported herein.

2. Materials and methods

2.1. Material

PEGT/PBT co-polymers were obtained from IsoTis S.A. (Bilthoven, The Netherlands) with a composition denoted as $a/b/c$, where a represents the PEG molecular weight (MW), and b and c represent the weight percentage (wt%) of the PEGT and PBT blocks, respectively. Co-polymer compositions of hydrophobic 300/55/45 and hydrophilic 1000/70/30 were chosen for use in this study based on previous work indicating their suitability for chondrocyte attachment and tissue formation [3,7,31,32].

The mechanical properties of these co-polymer compositions have been determined previously from dense tensile test specimens [23]. The tensile modulus (E) and tensile strength (σ) for 300/55/45 co-polymer compositions were 187.5 ± 5.0, 15.3 ± 0.4 MPa, respectively, while for 1000/70/30 co-polymers were shown to be 33.95 and 5.27 MPa, respectively.

2.2. 3D-deposition process

Porous 3D scaffolds were constructed using a custom designed fiber-deposition device consisting of five main components; (1) a thermostatically controlled heating jacket; (2) a molten co-polymer dispensing unit consisting of a syringe and nozzle; (3) a force-controlled plunger to regulate flow of molten co-polymer (4); a stepper motor driven $x-y-z$ table; and (5) a positional control unit consisting of stepper-motor drivers linked to a personal computer containing software for generating fiber deposition paths (Fig. 1).

The stainless steel heating jacket contained four thermostatically controlled heating rods capable of evenly conducting heat (from 0°C to 350°C) to a stainless steel syringe placed within the heating jacket. Co-polymer granules were placed in the syringe purged with nitrogen gas and allowed to melt. A stainless steel plunger with a teflon seal was used to apply pressure to the molten polymer. Pressure was regulated by placing the entire deposition device beneath the crosshead of a standard tension-compression test machine (Hounsfield HTE) in order to control the displacement of the plunger and monitor the resultant force (detected by a 20 kN load cell). Therefore, accurate control over the flow rate of polymer from the nozzle of the syringe was obtained. The nozzles were custom designed, and constructed by brazing medical grade syringe needles of varying diameter (e.g., 150, 250, and 350 μm inside diameter) onto a threaded, conical stainless steel tip.

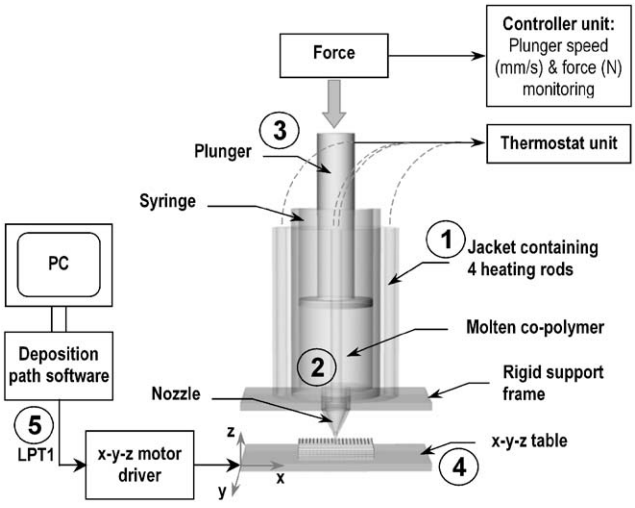

Fig. 1. The 3D deposition device consisted of five main components: (1) a thermostatically controlled heating jacket; (2) a molten co-polymer dispensing unit consisting of a syringe and nozzle; (3) a force-controlled plunger to regulate flow of molten co-polymer (4); a stepper motor driven $x-y-z$ table; and (5) a positional control unit consisting of stepper-motor drivers linked to a personal computer containing software for generating fiber deposition paths.

Stepper motors (Saia-Burgess AG, Switzerland) co-ordinated speed and translation of the $x-y-z$ table (Proxxon GmbH, Germany), and were controlled by a custom deposition program (designed using Visual Basic, Microsoft Corporation) via the printer port (LPT1). The program required inputs of the overall scaffold dimensions, the spacing between deposited fibers, the number of fiber layers, and the speed at which the $x-y-z$ table translated (Table 1). By lowering the $x-y$ table one layer-step in the z-direction, successive layers of rapidly solidifying fibers were laminated to previous layers in a 0°–90° pattern creating a consistent pore size and 100% interconnecting pore volume (Fig. 2). Fiber layers could be continuously deposited resulting in scaffolds up to 10 mm thick in some cases; however, in general, scaffolds 4 mm thick were created for cell culture experiments. These dimensions were chosen given that 4 mm is approximately the thickness of the cartilage layer present in human articular knee cartilage [34,35] and also presented challenging dimensions with which to assess in vitro and in vivo cartilage formation.

For cell culture experiments, cylindrical samples were cored from 4 mm thick blocks. Prior to cell seeding, scaffolds were incubated in isopropanol overnight to remove contaminants before being allowed to air-dry, with a further drying step overnight in a vacuum oven at 50°C. Scaffolds were then sterilized by gamma irradiation (minimum dose 25 kGy) in a JS6500 Tote Box Irradiator at Isotron B.V. (Ede, The Netherlands).

2.3. Characterization

Owing to the regular pore geometry, determining the interconnecting pore size of the resulting scaffolds was possible using scanning electron microscopy (SEM). The theoretical volume percent (vol%) porosity was calculated for each scaffold using deposition geometries based on a unit cube, whereby the fiber diameter and spacing between layers were equal (i.e., no overlap due to the fusion between fibers from one layer to another was assumed).

$$\text{Vol\% porosity}_{\text{theoretical}} = \left(1 - \frac{V_f}{V_c}\right) \times 100\%. \quad (1)$$

Here

$$V_f = \text{scaffold fiber volume (mm)}^3 = \frac{\pi d^2 L n_1 n_2}{4}$$

Table 1
Processing parameters for 3D deposited scaffolds

Sample	Fiber deposition temperature (°C)	Nozzle diameter (μm)	Applied force (kN)	Crosshead speed (mm/min)	$x-y-z$ table speed (mm/s)	$x-y$ fiber spacing (mm)	z fiber spacing (mm)
300/55/45–1.0 mm	200	250	2.0	0.4	5	1.0	0.2
300/55/45–1.0 mm stag	200	250	2.0	0.4	5	1.0	0.2
300/55/45–2.0 mm	200	250	2.0	0.4	5	2.0	0.2
1000/70/30–0.5 mm	180	250	1.5	0.2	5	0.5	0.2
1000/70/30–1.0 mm	180	250	1.5	0.2	5	1.0	0.2
1000/70/30–1.0 mm stag	180	250	1.5	0.2	5	1.0	0.2

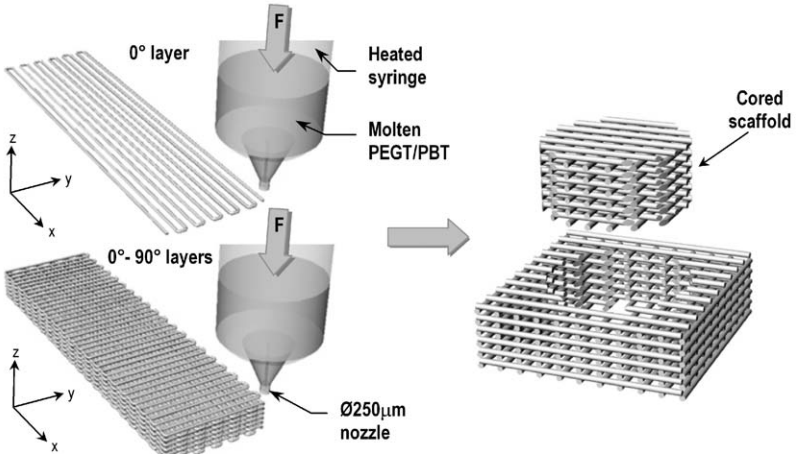

Fig. 2. 3D deposition process where ∅250 μm PEGT/PBT fibers are successively laid down in a computer controlled pattern (0–90° orientation shown). Scaffolds are subsequently cored from the deposited bulk material.

and

V_c = total scaffold cube volume $(\text{mm})^3 = Lwh$.

Therefore,

$$\text{Vol\% porosity}_{\text{theoretical}} = \left(1 - \frac{\pi d^2 n_1 n_2}{4wh}\right) \times 100\%, \quad (2)$$

where d, L, w, and h refer to the fiber diameter, fiber length, scaffold width, and scaffold height in millimeters, respectively. Furthermore, n_1 represents the number of fibers per layer, while n_2 represents the number of layers per scaffold.

Vol% porosity was also measured using mass/volume techniques according to the following relationship:

$$\text{Vol\% porosity}_{\text{measured}} = \left(1 - \frac{V_s}{V_c}\right) \times 100\%. \quad (3)$$

Here

V_s = apparent scaffold volume $(\text{mm}^3) = \dfrac{m}{\rho}$

and

V_c = total scaffold cube volume $(\text{mm}^3) = Lwh$.

Therefore,

$$\text{Vol\% porosity}_{\text{measured}} = \left(1 - \frac{m}{\rho Lwh}\right) \times 100\%, \quad (4)$$

where m represents the mass of the scaffold (g) and ρ represents the co-polymer density (g/mm^3), whereby, $\rho_{300/55/45}$ equals 1.25×10^{-3} g/mm^3 and $\rho_{1000/70/30}$ equals 1.20×10^{-3} g/mm^3. Owing to the amphiphilic nature of the PEGT/PBT co-polymers, the degree of swelling was determined by measuring the percentage change in diameter (mm) between dry scaffolds and scaffolds incubated at 37°C for 24 h in a phosphate buffered saline (PBS) solution.

2.4. Differential scanning calorimetry (DSC)

Differential scanning calorimetry (DSC Pyris 1, Perkin Elmer) was used to determine the thermal response of the co-polymers pre- and post-processing. Samples (7.5–14.0 mg) of 300/55/45 and 1000/70/30 resin and 3D-deposited scaffolds produced after 1 h of fiber deposition were heated from 80°C to 250°C at a rate of 10°C/min in aluminum pans with nitrogen as a

purge gas. The resulting DSC curves were analyzed to determine melting (T_m) and crystallization (T_c) temperatures of the more crystalline PBT component.

2.5. Intrinsic viscosity (IV)

Intrinsic viscosity was measured to give an indication of relative changes in molecular weight (MW) of the co-polymer pre- and post-processing [36]. The intrinsic viscosity (η) of 300/55/45 and 1000/70/30 resins and 3D-deposited scaffolds produced after 1 h of fiber deposition were determined from a solution of 0.5 g/dl of co-polymer in chloroform ($CHCl_3$) using a Schott Gerâte Ubbelohde viscometer (DIN type 0c) at 25°C.

2.6. Mechanical evaluation

Scaffolds: ∅4 mm × 4 mm thick cylinders were cored from 3D-deposited blocks and soaked overnight in phosphate buffered saline (PBS, Sigma) to allow for hydration and swelling. Samples were then placed in a PBS bath at room temperature between two compression plates of a Zwick Z050 tension-compression machine. The unconfined equilibrium modulus was determined by applying a step displacement (20% strain) and monitoring compressive force with time until equilibrium was reached (approximately 900 s). The ratio of equilibrium force to cross-sectional area was divided by the applied strain to calculate the equilibrium modulus (in MPa). Dynamic stiffness properties were determined by applying unconfined cyclic compression between 5% and 20% strain at a frequency of 0.1 Hz until an equilibrium force amplitude was observed (typically 50 cycles). Dynamic stiffness (in MPa) was calculated by taking the ratio of average force amplitude for the last 10 cycles to cross-sectional area, and dividing by the applied strain.

Articular Cartilage: Osteochondral plugs ∅4 mm were cored from the trochlear groove of 6-month old bovine knee joints. Articular cartilage cylinders, 4 mm thick, were obtained using a custom designed holder that allowed perpendicular sections to be accurately made. Samples were then immediately placed in PBS at room temperature for 3–4 h to equilibrate. The equilibrium modulus (at 20% strain) and dynamic stiffness (at 0.1 Hz) were determined as above for the scaffolds; however, a greater number of cycles were necessary to reach an equilibrium force amplitude for dynamic stiffness measurements (typically 100 cycles).

2.7. Tissue culture

Bovine: For seeding and culture of bovine chondrocytes, 3D deposited scaffolds were produced using a 300/55/45 co-polymer composition and a 1 mm fiber spacing (Fig. 3a and b). Chondrocytes were isolated via collagenase digestion from articular cartilage harvested from medial and lateral condyles of freshly slaughtered 6-month old bovine knee joints. Primary cells were dynamically seeded in spinner flasks (100 ml working volume, 50 rpm) on ∅7 mm by 4 mm thick scaffolds for 3 days at a density of 8×10^6 cells per scaffold. The culture medium contained HEPES (Gibco-BRL)-buffered DMEM (Gibco-BRL) supplemented with 10% fetal bovine serum (FBS, Sigma-Aldrich), 0.2 mM ascorbic acid 2-phosphate (Invitrogen), 0.1 mM non-essential amino acids (Sigma-Aldrich), 0.4 mM proline (Sigma-Aldrich), 100 units/ml penicillin (Gibco-BRL), and 100 μg/ml streptomycin (Gibco-BRL). The scaffolds were then dynamically cultured in spinner flasks for 21 days in the same medium, which was refreshed every 3–4 days.

To access the ability of scaffolds to support chondrogenesis in vivo, smaller ∅4 mm by 4 mm thick

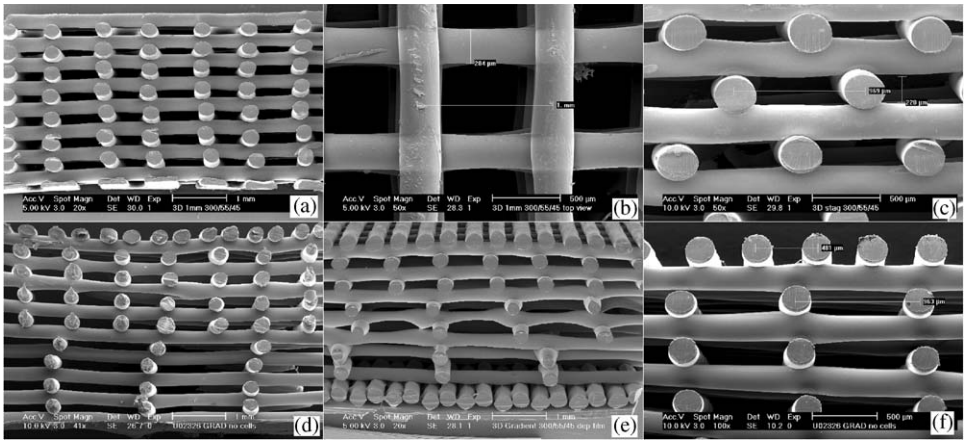

Fig. 3. SEM sections of 3D deposited scaffolds with varying fiber deposition geometries; (a) homogeneous 1 mm fiber spacing showing typical fiber diameters and pore geometries × 20, (b) top view × 50; (c) 1 mm staggered fiber spacing × 50; (d) inhomogeneous pore-size gradient × 20; (e) inhomogeneous pore-size gradient deposited on dense basal layer of fibers × 20; (f) superficial layer of gradient scaffold × 50.

scaffolds were seeded dynamically (as described above) for 7 days at a cell density of 3×10^6 cells per scaffold (i.e. the same cell density/mm^2 as the larger in vitro scaffolds). Scaffolds were subsequently implanted in subcutaneous pockets of 6-week old nude mice (HdCpb:NMRI-nu, Harlan, The Netherlands). Animals were sacrificed at 21 days after implantation, and constructs were processed histologically as described below.

Human: 3D deposited scaffolds for seeding of expanded human articular chondrocytes were also produced from 300/55/45 co-polymers with a 1 mm fiber spacing; however, the spacing of fibers was staggered between successive layers (Fig. 3c). Human articular chondrocytes were isolated via collagenase digestion of biopsies obtained from patients undergoing hip replacement surgery and culture-expanded in monolayer until passage 2. The cells were then trypsinized and dynamically seeded in spinner flasks (as described above) on Ø4 mm by 4 mm thick scaffolds for 5 days at a density of 3×10^6 cells/scaffold using the same above-mentioned culture medium, and without the use of additional growth factors.

2.8. Evaluation

Histology: Samples were fixed overnight in 0.14 M cacodylate buffer (pH = 7.2–7.4) containing 0.25% glutaraldehyde (Merck). Samples were then dehydrated in sequential ethanol series, plastic embedded in glycol-methacrylate (Merck) and cut using a microtome to yield 5 μm thick sections. Sections were stained with haematoxylin (Sigma-Aldrich) and fast green (Merck) to visualize cells/cell nuclei and counterstained with safranin-O (Sigma-Aldrich) to visualize extracellular glycosaminoglycans (GAG). Mounted slides were examined under a light microscope (Nikon Eclipse E400) and representative images captured using a digital camera (Sony Corporation, Japan) and Matrix Vision software (Matrix Vision GmbH, Germany).

Scanning electron microscopy (SEM): Samples were fixed and dehydrated as described above and critical point dried from liquid carbon dioxide using a Balzers CPD 030 critical point dryer. Dried tissue-cultured samples or as-produced scaffolds were then sputter coated (Cressingdon) with a thin gold layer and studied using a Philips XL30 environmental scanning electron microscope (ESEM).

Immunohistochemistry: Constructs were embedded in optimal cutting temperature (OCT) compound (Tissue-Tek) and snap frozen at −60°C. Cryo-sections, 5 μm in thickness, were made (Cryotome, Thermo Shandon) and fixed in acetone for 8 min. Collagen type II was immuno-localized using an Animal Research Kit (Dako) in combination with a collagen type II antibody (1:200, II-II6B3, Developmental Studies Hybridoma Bank). In brief, after digestion for 20 min with 0.025% trypsin-EDTA (Gibco) at room temperature, samples were rinsed with PBS (Gibco) and incubated with peroxidase block for 5 min. Samples were then incubated with a biotinylated primary antibody for 15 min, rinsed with PBS, followed by the application of streptavin-peroxidase for 15 min. After rinsing with PBS, the staining was visualized using DAB-solution for 5 min in addition to counter staining with haematoxylin (Sigma). Samples were examined under a light microscope (Nikon Eclipse E400) and representative images captured using a digital camera (Sony Corporation, Japan) and Matrix Vision software (Matrix Vision GmbH, Germany).

Cell viability: A live/dead assay (Molecular Probes) was used to access cell viability. Ethidium-bromide homodimer was used as a marker for dead cells due to the fact that it binds fragmented deoxyribonucleic acid (DNA) in cells that no longer have an intact plasma membrane, and fluoresces red. Calcein AM is capable of permeating the plasma membrane of viable cells, where it is cleaved by intracellular esterases and fluoresces green [37]. Constructs were harvested and 1 mm thick sections incubated in a PBS solution containing 6 μmol/l ethidium bromide homodimer and 2 μmol/l calcein AM for 30 min at 37°C. Sections were examined in an inverted fluorescent microscope (Nikon Eclipse E400) using an FITC Texas Red filter. Representative images were captured using a digital camera (Sony Corporation, Japan) and Matrix Vision software (Matrix Vision GmbH, Germany).

3. Results and discussion

3.1. Characterization

SEM analysis confirmed that 3D deposited scaffolds consisted of 100% interconnecting pores (Fig. 3a–d, and f). Only in scaffold designs where the fiber spacing was controlled to deliberately produce completely dense layers (as illustrated in the pore gradient scaffolds in Fig. 3e) was interconnectivity compromised. By varying the deposition path (e.g., the fiber spacing) and accurately controlling deposition parameters (e.g., temperature, syringe pressure, $x-y-z$ table velocity), a range of scaffold architectures were produced from 300/55/45 and 1000/70/30 PEGT/PBT co-polymer compositions. Scaffolds contained smooth fibers approximately 250 μm in diameter and, with a fiber spacing ranging between 0.5 and 2.0 mm, average interconnecting pore sizes in the $x-y$ plane ranged between ~150 and ~1650 μm, respectively, as shown by SEM analysis (Table 2). Average interconnecting pore size in the z-plane was related to the fiber diameter, and ranged between 170 and 195 μm irrespective of fiber spacing.

Table 2
Structural characterization of deposited scaffolds

Sample	Theoretical pore size		Avg. interconnecting pore size		Swelling (%)	Theoretical vol% porosity (%)	Measured vol% porosity (%)
	$x-y$ plane (μm)	z-plane (μm)	$x-y$ plane (μm)	z-plane (μm)			
300/55/45–1.0 mm	750	200	646±65	185±52	2.1±1.2	78.0	70.8±1.77
300/55/45–1.0 mm stag	750	200	610±20	180±22	1.8±0.1	78.0	70.2±1.16
300/55/45–2.0 mm	1750	200	1653±91	171±27	2.0±0.6	87.4	87.4±0.43
1000/70/30–0.5 mm	250	200	150±38	195±21	17.7±2.4	59.2	55.4±0.93
1000/70/30–1.0 mm	750	200	652±49	188±30	18.7±2.6	78.0	71.5±1.13
1000/70/30–1.0 mm stag	750	200	616±33	177±46	16.8±2.0	78.0	71.5±1.81

Table 3
Intrinsic viscosity and thermal characterization of deposition process

Sample	Intrinsic viscosity η (dl/g)	Melting temp $T_{m\,PBT}$ (°C)	Enthalpy of fusion ΔH_{PBT} (J/g)	Crystallization temp $T_{c\,PBT}$ (°C)
300/55/45 resin	0.68±0.03	151.4±2.7	19.5±4.4	95.6±3.5
300/55/45 scaffold	0.66±0.01	156.5±3.2	22.8±5.5	103.4±3.6
1000/70/30 resin	0.80±0.01	149.8±3.0	13.2±1.8	106.1±10.3
1000/70/30 scaffold	0.79±0.01	155.8±4.8	12.0±7.0	116.0±12.3

During deposition, molten PEGT/PBT co-polymers fibers rapidly solidified resulting in a continuous bond with the underlying fibers and, hence, a solid fusion between scaffold layers (Fig. 3a–f).

Owing to the higher wt% PBT content and, thus, more hydrophobic nature of 300/55/45 co-polymers, swelling in scaffolds produced using this composition was limited to an increase of approximately 2.0%. Conversely, the more hydrophilic 1000/70/30 co-polymers showed an increase in swelling by approximately 18% (Table 2).

Theoretical volume percent porosity based on deposition paths ranged between 59.0% and 87.4%. However, due to the fusion between fibers and the underlying layers, measured porosity values were somewhat less, as has been shown during 3D dispensing of hydrogel materials [22]. These differences can be further explained by the fact that the theoretical calculations assume a unit cube as opposed to the actual continuous strand of fiber, which generated edge effects. Minor deviations in fiber diameter and deposition geometry also likely make a contribution.

3.2. Intrinsic viscosity and thermal characterization

There was no significant increase in IV of deposited scaffolds compared with co-polymer resin indicating the 3D deposition process did not significantly alter the relative MW of both 300/55/45 and 1000/70/30 co-polymers (Table 3). DSC analysis of thermal properties resulted in a slightly higher melting temperature (T_m), enthalpy of fusion of the more crystalline PBT phase (ΔH_{PBT}), and crystallization temperature (T_c) for deposited scaffolds as compared with resin. This was likely due to differences in thermal history between resin processing and 3D deposition, rather than significant changes in co-polymer crystallinity. These results demonstrate that the processing parameters used did not induce changes in MW due to degradation at elevated temperatures or shear forces during fiber deposition, which in turn could compromise scaffold biocompatibility and/or biodegradation.

3.3. Mechanical properties

Under compression, articular cartilage behaves like a poroelastic material, whereby it's response to compressive loads are frequency and strain dependent, and is governed by the interrelationship between solid ECM constituents (e.g., collagen type II) and interstitial fluid flow (e.g., water) [38–40]. To characterize the mechanical properties of scaffolds with varying architecture and co-polymer composition, both static and dynamic compression tests were performed under wet conditions and compared with native articular cartilage tissue.

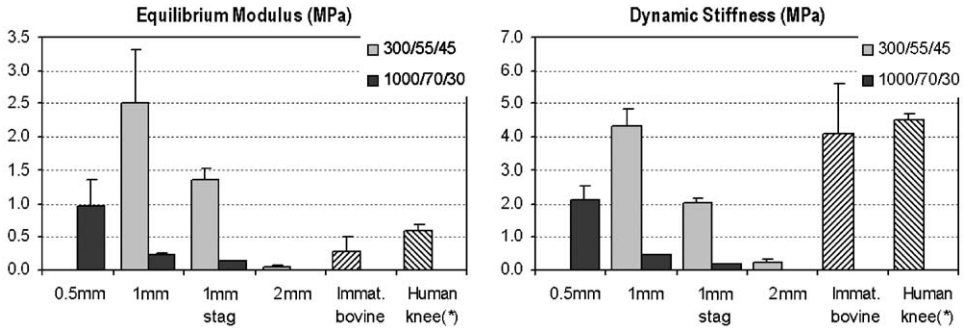

Fig. 4. Equilibrium modulus and dynamic stiffness (0.1 Hz) of hydrated 3D-deposited scaffolds compared with natural articular cartilage (* taken from [43]).

With respect to co-polymer composition, scaffolds deposited using 300/55/45 yielded higher equilibrium modulus and dynamic stiffness values as compared with 1000/70/30 scaffolds of the same geometry (Fig. 4). This was likely due to the lower PEG MW and greater wt% ratio of "hard" PBT blocks to "soft" PEGT blocks present in the 300/55/45 scaffolds, and limited water uptake. Similar mechanical behavior has been reported in tensile test specimens of PEGT/PBT co-polymers with the same composition [26].

Fig. 4 illustrates that by controlling scaffold architecture, the mechanical properties could also be influenced. In general, highly porous structures exhibit limited mechanical properties whereby a power-law exists relating porosity to compressive stiffness [14]. Similar behavior was seen in this study where scaffolds with reduced fiber spacing (e.g., 0.5 mm) and, thus, low vol% porosity (e.g., 59.0%) resulted in higher equilibrium modulus and dynamic stiffness as compared with scaffolds with larger fiber spacing (e.g., 2 mm) and high vol% porosity (e.g., 87%). It must be noted, however, that by altering the deposition pattern, the bulk mechanical properties of the scaffolds were changed. Therefore, equilibrium modulus and dynamic stiffness could not be directly correlated with scaffold porosity. For example the equilibrium modulus and dynamic stiffness of 1 mm staggered 300/55/45 and 1000/70/30 scaffolds (Fig. 3c) were approximately 50% of those values measured for scaffolds with a homogeneous 1 mm fiber spacing, even though they had almost identical vol% porosity (see Table 2). This was due to the fact that, under compression, the homogeneous 1 mm spaced scaffolds with fibers lying directly underneath each other presented stiffer columns of fibers compared with staggered scaffolds where fibers, in any given layer, never lay directly underneath one another.

In natural cartilage tissue, unconfined compression testing of bovine articular cartilage explants resulted in an equilibrium modulus and dynamic stiffness (at 0.1 Hz) of 0.27 and 4.10 MPa, respectively. These values compare favorably with previous unconfined compression studies on bovine articular cartilage [41,42]. Only 300/55/45 scaffolds with a 2 mm fiber spacing and 1000/70/30 scaffolds with both 1 and 1 mm staggered spacing had equilibrium modulus values equal-to or less-than bovine articular cartilage. When tested under dynamic compression, 300/55/45 scaffolds with 0.5 and 1.0 mm spacing most closely resembled those of native cartilage compared with scaffolds deposited from 1000/70/30 co-polymers.

The equilibrium modulus and dynamic stiffness (at 0.1 Hz) values cited in literature for human articular knee cartilage tested under confined compression are 0.6 and 4.5 MPa, respectively [43]. Although unconfined compression tests were performed in this study, which tend to underestimate values measured via confined compression, the mechanical data obtained in this study suggest that it is possible to design 3D deposited PEGT/PBT scaffolds which match the static and dynamic properties of articular cartilage, and thus be capable of supporting in vivo loading conditions within the human knee joint. While other investigators have reported the development of scaffolds with similar compressive modulus to articular cartilage [44], the development of scaffolds with similar dynamic stiffness properties to articular cartilage has not been reported previously. Given the frequency-dependant response of articular cartilage under compression, we postulate that the dynamic, rather than static, properties of articular cartilage may provide a more appropriate benchmark with which to emulate into scaffolds designed for articular cartilage repair. In future studies, we intend to evaluate in more detail the mechanical response of 3D-deposited scaffolds over and larger range of dynamic frequencies.

3.4. Tissue culture

SEM sections following 3 days dynamic seeding showed rapid cell/cell-aggregate attachment onto, and throughout, the PEGT/PBT scaffolds (Fig. 5a). Under these conditions, the early onset of chondrogenesis was

promoted as seen in safranin-O sections where newly synthesized ECM stained positively for GAG (Fig. 5b). There was near-complete formation of cartilage-like tissue within the interconnecting pores after 21 days dynamic culture (Fig. 5c). Again, positive GAG staining was observed throughout, even in ECM synthesized deep within the ∅7 mm by 4 mm thick scaffold (Fig. 5d). Similar to previous reports studying dynamic culture of cartilagenous constructs in vitro [45,46], a thin capsule of fibroblast-like cells was observed surrounding the periphery of the scaffold. This was highlighted in immuno-sections where the peripheries of the constructs positively expressed collagen type I, which is synthesized by cells with a fibroblastic phenotype (Fig. 5e). In contrast, collagen type II, which is synthesized by cells with a chondrocytic phenotype, was predominantly expressed throughout the interior of the constructs (Fig. 5f), and was in accordance with the GAG staining observed in safranin-O sections.

Subcutaneous implantation of ∅4 mm by 4 mm thick scaffolds, dynamically cultured for 7 days, resulted in even greater tissue formation than in vitro samples, as observed qualitatively from SEM and safranin-O sections (Fig. 5g and h). ECM exhibiting a cartilage-like morphology was observed throughout the scaffold and stained positively for GAG even beyond the border of

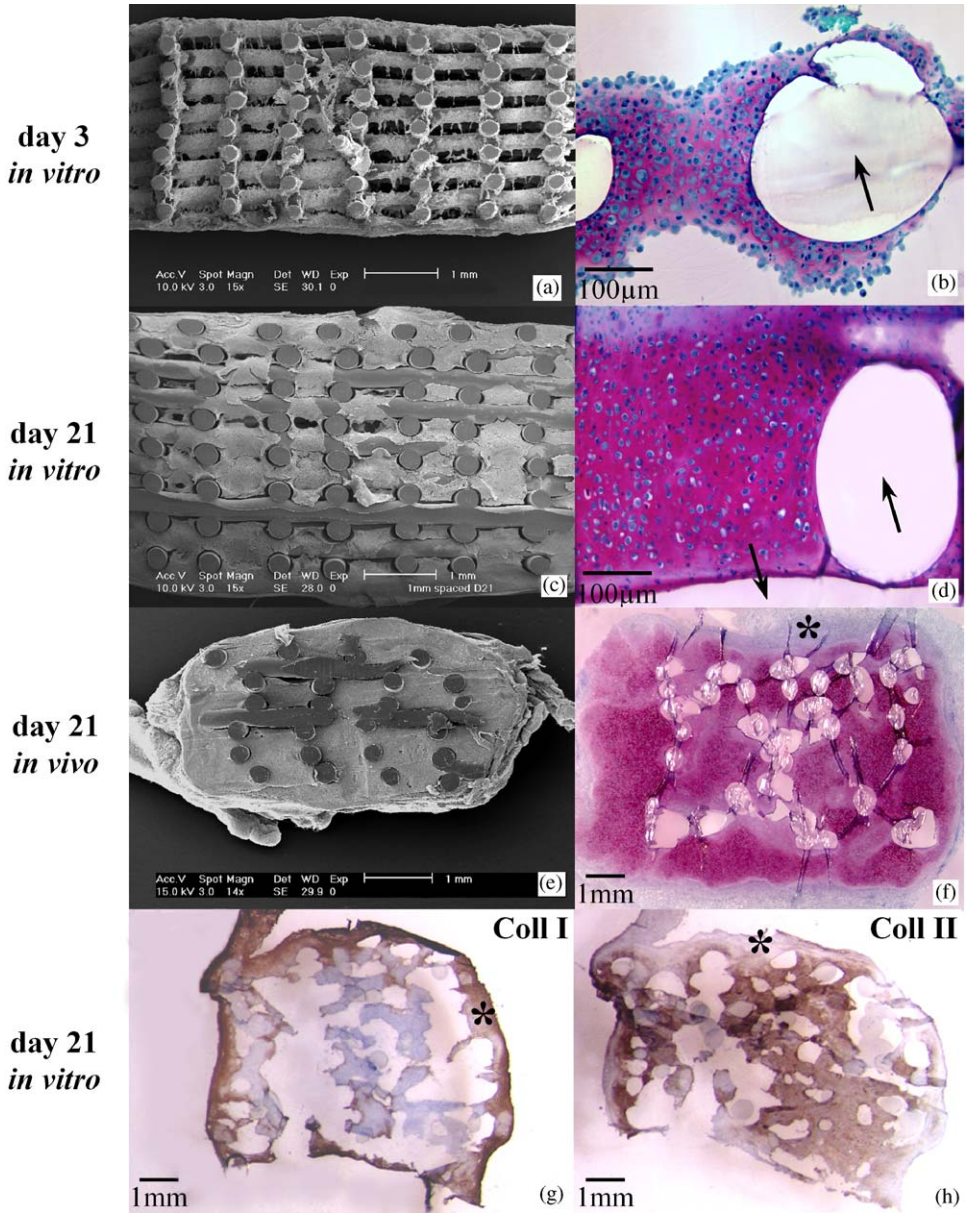

Fig. 5. SEM (a, c, e × 15), safranin-O stained (b, d, f), and collagen type-I and type-II immunohistochemistry sections (g, h) of 3D-deposited 300/55/45 scaffolds following (a, b) 3 days dynamic seeding of bovine articular chondrocytes; (c, d, g, h) 21 days dynamic culture in vitro; (e, f) 21 days subcutaneous implantation in nude mice; (arrows indicate PEGT/PBT fiber, * indicates fibrous capsule).

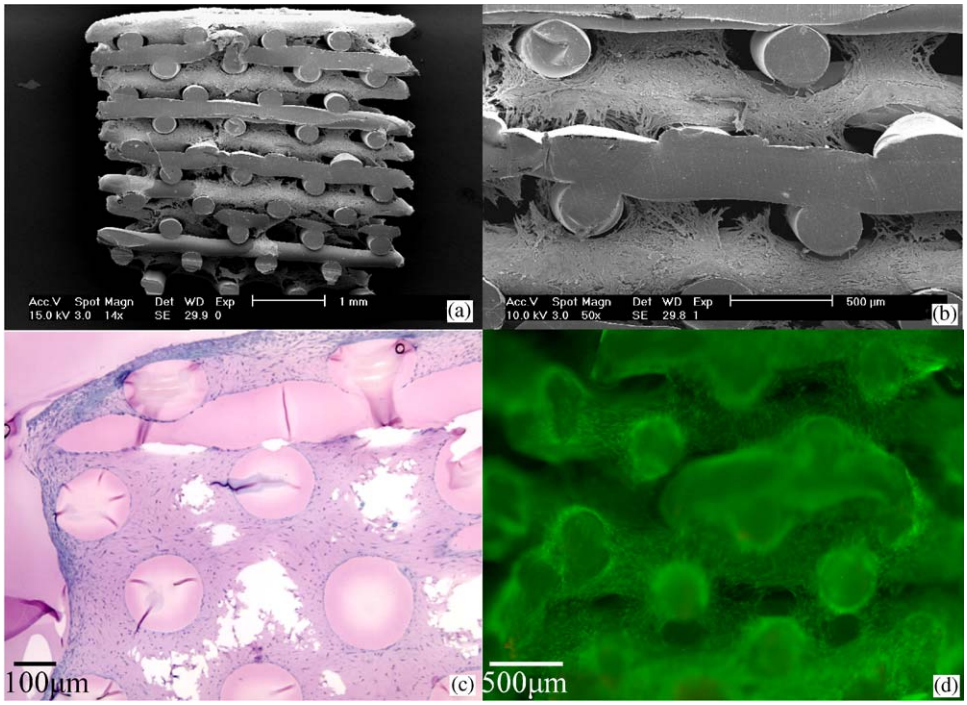

Fig. 6. SEM (a × 15, b × 50), safranin-O (c), and live/dead (d) sections showing attachment, proliferation and high percentage of live (green) expanded human articular chondrocytes throughout interconnecting pores on 3D-deposited 300/55/45 scaffolds following 5 days dynamic seeding.

the scaffold fibers. Again, at the very periphery of the construct, a fibrous capsule was present.

Although bovine chondrocytes, which typically exhibit a higher metabolic activity as compared to human chondrocytes [47], were used in this evaluation study, the rapid chondrogenesis observed may further be attributed to the large number of cell-cell interactions as well as enhanced nutrient exchange provided by the highly accessible and interconnecting pore structure in addition to the dynamic flow conditions [48–50].

A preferable cell source for scaffold-based strategies to repair clinically sized articular cartilage defects are human articular chondrocytes, which are typically culture expanded in monolayer to yield sufficient quantities for seeding [7]. In this study, seeding of expanded (passage 2) human articular chondrocytes resulted in rapid cell attachment and proliferation as indicated by multiple layers of elongated cells observed in SEM and safranin-O sections at day 5 (Fig. 6a–c). Furthermore, tissue was beginning to bridge the interconnecting pores between the staggered fibers (Fig. 6c), and contained a high percentage of living cells as observed in fluorescent live/dead stained sections (Fig. 6d).

3.5. 3D-deposition process

While the intent was that the 3D deposition device be adapted to an RP system in the future, thus allowing complex 3D geometries to be developed from CAD/CAM design and control of fiber deposition, our initial goal was the development of simple geometries with controlled and repeatable pore architectures in order to study tissue formation. In the development of 3D-deposited scaffolds, it is important to discuss the critical processing parameters.

If we assume the molten co-polymer to be a viscous Newtonian fluid (i.e., non-compressible) with a parabolic flow profile (i.e., when nozzle length = 6x nozzle diameter), the flow rate from the nozzle can be expressed according to the Hagen–Poiseuille equation [20]:

$$Q = \frac{\pi \Delta P}{128 L \eta} d^4. \tag{5}$$

As shown in Eq. (5), the flow rate (Q) of the co-polymer is directly proportional to both the pressure differential (ΔP) across the syringe and nozzle tip, and the nozzle diameter (d), while both Q and ΔP are inversely proportional to nozzle length (L) and co-polymer viscosity (η). Controlling co-polymer flow rate is critical as a high Q resulted in over-deposition of the fiber, causing draping between fibers and reducing porosity, whereas a low Q will reduce the fiber diameter, thus compromising contact between the underlying fibers and overall scaffold integrity. Changes in Q could be buffered by controlling $x-y-z$ table velocity, thus adjusting the take-off speed of fiber from the nozzle. Furthermore, minor decreases in nozzle diameter will dramatically decrease flow rate and require considerably

greater pressures to deposit suitable fibers, as will an increase in nozzle length to a lesser extent. For very small nozzle diameters (i.e., $<100\,\mu m$), the pressures required to achieve a suitable flow rate can be beyond those practically possible, necessitating changes in viscosity. Addition of solvents, such as chloroform [19,20], or increasing the syringe temperature to reduce the co-polymer viscosity would assist deposition of fibers at small nozzle diameters. However, incomplete removal of solvents post-processing and exposure of polymers to excessive oxidation at elevated temperatures can be detrimental to scaffold biocompatibility [8,21]. On a macroscopic level, a reduced fiber diameter would allow a higher scaffold resolution but would also result in a reduced pore size in the *z*-direction as well as increasing the processing time of thick scaffolds. One solution would be to deposit two layers of fibers in an identical pattern, directly on top of one other, thereby doubling the interconnecting pore size in the *z*-direction.

The 3D deposition device presented here was designed to eliminate these concerns by using a solvent-free processing technique and thermally stable co-polymers operating under a non-oxidizing nitrogen environment. As shown by IV and DSC analysis, PEGT/PBT co-polymer MW was not affected by the deposition process (Table 3). Furthermore, there was no shrinkage of scaffolds during processing, and hydrophilic compositions (i.e., 1000/70/30) of scaffold also allowed for swelling during subsequent culture. In addition to varying scaffold fiber spacing, nozzles and/or syringes could be interchanged during processing in the future in order to deposit fibers of different diameter, or co-polymers of different composition. This would allow considerable freedom with respect to the structural organization of scaffolds. For example, interconnecting pore size, fiber surface area, surface chemistry, degradation behavior and mechanical properties could be controlled from one layer to another. We already demonstrated in this study the ability to create anisotropic scaffolds containing pore-size gradients ranging from very small pores ($\sim 150\,\mu m$) to very large pores ($\sim 1650\,\mu m$) throughout the depth of the construct (Fig. 3d and f).

4. Conclusions

We have presented and characterized a fiber deposition technique for producing 3D scaffolds with a well defined, and 100% interconnecting, pore network for engineering of articular cartilage. The 3D deposition technique allowed us to "design-in" desired scaffold characteristics, such as porosity, pore size and mechanical properties using computer-controlled tooling processes. Using two PEGT/PBT co-polymer compositions, and by changing the spacing between deposited fibers from one layer to another, a range of scaffold geometries were created, including scaffolds with a staggered fiber spacing; scaffolds with pore size gradients with height; and scaffolds with complete dense layers (Fig. 3).

Fiber-based scaffolds were generated from two different PEGT/PBT co-polymers compositions, a hydrophobic 300/55/45 and hydrophilic 1000/70/30, with varying swelling capabilities ranging between 2% and 18%, respectively. Static and dynamic mechanical compression showed differences in equilibrium modulus and dynamic stiffness ranging from 0.05–2.5 to 0.16–4.33 MPa, respectively, based on co-polymer composition and scaffold porosity. Furthermore, by maintaining a consistent vol% porosity, mechanical properties could be influenced by manipulating scaffold geometry (e.g., a homogenous fiber spacing as compared to a staggered fiber spacing between layers). Scaffolds constructed from 300/55/45 co-polymer fibers with a 1 mm spacing and porosity of 71% resulted in a similar dynamic stiffness values compared with bovine and human articular cartilage tested at a frequency of 0.1 Hz. Thermal characterization (DSC and IV analysis) showed that relative co-polymer MW was not significantly altered during processing compared with PEGT/PBT resin.

3D-deposited scaffolds supported rapid attachment of bovine chondrocytes and tissue formation following dynamic culture in vitro and subcutaneous implantation in nude mice as demonstrated by the presence articular cartilage ECM constituents, GAG and type II collagen, throughout the interconnected interior pore volume. Similar results were achieved with respect to the attachment of expanded human articular chondrocytes, resulting in a homogenous distribution of viable cells after 5 days dynamic seeding.

The processing methods and model scaffolds developed in this study provide an elegant method to further investigate the effects of scaffold composition and pore architecture on cartilage tissue formation in vitro or under load bearing conditions in vivo.

Acknowledgements

The authors would like to acknowledge funding from the European Commission (FP5 project "Scafcart" G5RD-CT-1999-00050).

References

[1] Mankin HJ, Mow VC, Buckwalter JA, Iannotti JP, Ratcliffe A. Articular cartilage structure, composition and function. In: Buckwalter JA, Einhorn TA, Simon SR, editors. Orthopaedic basic science: biology and biomechanics of the musculoskeletal

system. Rosemont, IL: American Academy of Orthopaedic Surgeons; 2000. p. 443–70.
[2] Mankin HJ, Mow VC, Buckwalter JA. Articular cartilage repair and osteoarthritis. In: Buckwalter JA, Einhorn TA, Simon SR, editors. Orthopaedic basic science: biology and biomechanics of the musculoskeletal system. 2nd ed. Rosemont, IL: American Academy of Orthopaedic Surgeons; 2000. p. 471–88.
[3] Hunziker EB. Articular cartilage repair: basic science and clinical progress. A review of the current status and prospects. Osteo Cart 2002;10(6):432–63.
[4] Hunziker EB. Articular cartilage repair: are the intrinsic biological constraints undermining this process insuperable? Osteo Cart 1999;7(1):15–28.
[5] Solchaga LA, Goldberg VM, Caplan AI. Cartilage regeneration using principles of tissue engineering. Clin Orthop 2001; 391(Suppl):S161.
[6] Grande DA, Breitbart AS, Mason J, Paulino C, Laser J, Schwartz RE. Cartilage tissue engineering: current limitations and solutions. Clin Orthop 1999;367(Suppl):S176.
[7] Woodfield TBF, Bezemer JM, Pieper JS, van Blitterswijk CA, Riesle J. Scaffolds for tissue engineering of cartilage. Crit Rev Eukaryot Gene Expr 2002;12(3):209–36.
[8] Hutmacher DW. Scaffolds in tissue engineering bone and cartilage. Biomaterials 2000;21(24):2529–43.
[9] Lu L, Zhu X, Valenzuela RG, Currier BL, Yaszemski MJ. Biodegradable polymer scaffolds for cartilage tissue engineering. Clin Orthop 2001;391(Suppl):S251.
[10] Yang S, Leong KF, Du Z, Chua CK. The design of scaffolds for use in tissue engineering. Part I. Traditional factors. Tissue Eng 2001;7(6):679–89.
[11] Yang S, Leong K, Du Z, Chua C. The design of scaffolds for use in tissue engineering. Part II. Rapid prototyping techniques. Tissue Eng 2002;8(1):1–11.
[12] Hutmacher DW. Scaffold design and fabrication technologies for engineering tissues—state of the art and future perspectives. J Biomater Sci Polym Ed 2001;12(1):107–24.
[13] Lu L, Mikos A. The importance of new processing techniques in tissue engineering. MRS Bull 1996;21(11):28–32.
[14] Zein I, Hutmacher DW, Tan KC, Teoh SH. Fused deposition modeling of novel scaffold architectures for tissue engineering applications. Biomaterials 2002;23(4):1169–85.
[15] Sun W, Lal P. Recent development on computer aided tissue engineering—a review. Comput Methods Programs Biomed 2002; 67(2):85–103.
[16] Hutmacher DW, Schantz T, Zein I, Ng KW, Teoh SH, Tan KC. Mechanical properties and cell cultural response of polycaprolactone scaffolds designed and fabricated via fused deposition modeling. J Biomed Mater Res 2001;55(2):203–16.
[17] Huang Q, Goh J, Hutmacher D, Lee E. In vivo mesenchymal cell recruitment by a scaffold loaded with transforming growth factor beta1 and the potential for in situ chondrogenesis. Tissue Eng 2002;8(3):469–82.
[18] Landers R, Hubner U, Schmelzeisen R, Mulhaupt R. Rapid prototyping of scaffolds derived from thermoreversible hydrogels and tailored for applications in tissue engineering. Biomaterials 2002;23(23):4437–47.
[19] Vozzi G, Flaim C, Ahluwalia A, Bhatia S. Fabrication of PLGA scaffolds using soft lithography and microsyringe deposition. Biomaterials 2003;24(14):2533–40.
[20] Vozzi G. Microsyringe-based deposition of two-dimensional and three-dimensional polymer scaffolds with a well-defined geometry for application to tissue engineering. Tissue Eng 2002;8(6): 1089–98.
[21] Landers R, Mulhaupt R. Desktop manufacturing of complex objects, prototypes and biomedical scaffolds by means of computer-assisted design combined with computer-guided 3D plotting of polymers and reactive oligomers. Macromolec Mater Eng 2000;282:17–21.
[22] Landers R, Pfister A, Hubner U, John H, Schmelzeisen R, Mulhaupt R. Fabrication of soft tissue engineering scaffolds by means of rapid prototyping techniques. J Mater Sci 2002;37(15): 3107–16.
[23] Sakkers RJB, de Wijn JR, Dalmeyer RAJ, Brand R, van Blitterswijk CA. Evaluation of copolymers of polyethylene oxide and poly buthylene terephthalate (Polyactive®): mechanical behaviour. J Mater Sci 1998;9:375–9.
[24] van Blitterswijk CA, van den Brink J, Leenders H, Bakker D. The effect of PEO ratio on degradation, calcification and bone-bonding of PEO/PBT copolymer (Polyactive). Cells Mater 1993; 3(23):23–36.
[25] Bezemer JM, Grijpma DW, Dijkstra PJ, van Blitterswijk CA, Feijen J. A controlled release system for proteins based on poly(ether ester) block-copolymers: polymer network characterization. J Controlled Release 1999;62(3):393–405.
[26] Deschamps AA, Claase MB, Sleijster WJ, de Bruijn JD, Grijpma DW, Feijen J. Design of segmented poly(ether ester) materials and structures for the tissue engineering of bone. J Controlled Release 2002;78(1-3):175–86.
[27] Radder AM, Leenders H, van Blitterswijk CA. Interface reactions to PEO/PBT copolymers (Polyactive) after implantation in cortical bone. J Biomed Mater Res 1994;28(2):141–51.
[28] Beumer GJ, van Blitterswijk CA, Bakker D, Ponec M. Cell-seeding and in vitro biocompatibility evaluation of polymeric matrices of PEO/PBT copolymers and PLLA. Biomaterials 1993;14(8):598–604.
[29] Radder AM, Leenders H, van Blitterswijk CA. Application of porous PEO/PBT copolymers for bone replacement. J Biomed Mater Res 1996;30(3):341–51.
[30] Beumer GJ, van Blitterswijk CA, Ponec M. Biocompatibility of a biodegradable matrix used as a skin substitute: an in vivo evaluation. J Biomed Mater Res 1994;28(5):545–52.
[31] Papadaki M, Mahmood T, Gupta P, Claase MB, Grijpma DW, Riesle J, van Blitterswijk CA, Langer R. The different behaviors of skeletal muscle cells and chondrocytes on PEGT/PBT block copolymers are related to the surface properties of the substrate. J Biomed Mater Res 2001;54(1):47–58.
[32] Mahmood TA. Chondrocyte–biomaterial interactions: a mechanistic approach to cartilage tissue engineering. PhD Thesis, University of Twente, Enschede, The Netherlands, 2003.
[33] Bezemer JM, Oude Weme P, Grijpma DW, Dijkstra PJ, van Blitterswijk CA, Feijen J. Amphiphilic poly(ether ester amide) multiblock copolymers as biodegradable matrices for the controlled release of proteins. J Biomed Mater Res 2000;52(1):8–17.
[34] Kladny B, Martus P, Schiwy-Bochat K, Weseloh G, Swoboda B. Measurement of cartilage thickness in the human knee joint by magnetic resonance imaging using a three-dimensional gradient echo sequence. Int Orthop 1999;23:264–7.
[35] Cicuttini FM, Wluka AE, Wang Y, Davis SR, Hankin J, Ebeling P. Compartment differences in knee cartilage volume in healthy adults. J Rheumatol 2002;29(3):554–6.
[36] Carraher CE. Polymer chemistry, 5th ed. New York: Marcel Dekker Inc; 2000.
[37] Haugland RP. Handbook of fluorescent probes and research chemicals, 7th ed. Eugene, OR: Molecular Probes; 1999.
[38] DiSilvestro MR, Zhu Q, Wong M, Jurvelin JS, Suh JK. Biphasic poroviscoelastic simulation of the unconfined compression of articular cartilage: I—simultaneous prediction of reaction force and lateral displacement. J Biomech Eng 2001;123(2):191–7.
[39] Li L, Buschmann M, Shirazi-Adl A. A fibril reinforced nonhomogeneous poroelastic model for articular cartilage: inhomogeneous response in unconfined compression. J Biomech 2000;33(12):1533–41.

[40] Li LP, Soulhat J, Buschmann MD, Shirazi-Adl A. Nonlinear analysis of cartilage in unconfined ramp compression using a fibril reinforced poroelastic model. Clin Biomech (Bristol, Avon) 1999;14(9):673–82.
[41] Jurvelin J, Buschmann M, Hunziker E. Optical and mechanical determination of Poisson's ratio of adult bovine humeral articular cartilage. J Biomech 1997;30(3):235–41.
[42] Korhonen R, Laasanen M, Toyras J, Rieppo J, Hirvonen J, Helminen H, Jurvelin J. Comparison of the equilibrium response of articular cartilage in unconfined compression, confined compression and indentation. J Biomech 2002;35(7):903–9.
[43] Treppo S, Koepp H, Quan EC, Cole AA, Kuettner KE, Grodzinsky AJ. Comparison of biomechanical and biochemical properties of cartilage from human knee and ankle pairs. J Orthop Res 2000;18(5):739–48.
[44] Niederauer GG, Slivka MA, Leatherbury NC, Korvick DL, Harroff HH, Ehler WC, Dunn CJ, Kieswetter K. Evaluation of multiphase implants for repair of focal osteochondral defects in goats. Biomaterials 2000;21(24):2561–74.
[45] Martin I, Obradovic B, Treppo S, Grodzinsky AJ, Langer R, Freed LE, Vunjak-Novakovic G. Modulation of the mechanical properties of tissue engineered cartilage. Biorheology 2000;37(1–2):141–7.
[46] Vunjak-Novakovic G, Martin I, Obradovic B, Treppo S, Grodzinsky AJ, Langer R, Freed LE. Bioreactor cultivation conditions modulate the composition and mechanical properties of tissue-engineered cartilage. J Orthop Res 1999;17(1):130–8.
[47] Kafienah W, Jakob M, Demarteau O, Frazer A, Barker M, Martin I, Hollander A. Three-dimensional tissue engineering of hyaline cartilage: comparison of adult nasal and articular chondrocytes. Tissue Eng 2002;8(5):817–26.
[48] Vunjak-Novakovic G, Obradovic B, Martin I, Freed L. Bioreactor studies of native and tissue engineered cartilage. Biorheology 2002;39(1,2):259–68.
[49] Malda J. Cartilage tissue engineering: the relevance of oxygen. PhD Thesis, University of Twente, Enschede, The Netherlands, 2003.
[50] Freed LE, Martin I, Vunjak-Novakovic G. Frontiers in tissue engineering. In vitro modulation of chondrogenesis. Clin Orthop 1999;367(Suppl):S46.